SCIENCE CHINA
Information Sciences

• RESEARCH PAPER •

September 2019, Vol. 62 192207:1–192207:14
https://doi.org/10.1007/s11432-018-9784-1

Hierarchical control for generator and battery in the more electric aircraft

Alberto CAVALLO*, Antonio RUSSO & Giacomo CANCIELLO

Department of Engineering, University of Campania, Aversa 81031*, Italy*

Received 9 November 2018/Accepted 31 January 2019/Published online 1 August 2019

Abstract This paper addresses the problem of intelligent power management for the more electric aircraft framework. The main objective is to regulate the power flow between a low voltage and a high voltage busses through control of a Buck-Boost converter unit. This approach allows the battery to help the generator when an overload scenario occurs, keeping at the same time the battery state of charge above a prescribed threshold. Moreover, in case a continued severe overload causes the battery state of charge to drop below a prescribed threshold, partial shedding of (noncritical) loads occurs. The control objectives are achieved through the design of a hierarchical control strategy based on high gain control for the low level and a finite state automaton for the high level control. Rigorous mathematical proofs of stability are provided for both low level and high level control and a detailed simulator with accurate model of the battery is presented in order to demonstrate the correctness and effectiveness of the proposed approach.

Keywords supervisory control, high gain control, sliding mode control, nonlinear control, robust control, more electric aircraft, switched systems

Citation Cavallo A, Russo A, Canciello G. Hierarchical control for generator and battery in the more electric aircraft. Sci China Inf Sci, 2019, 62(9): 192207, https://doi.org/10.1007/s11432-018-9784-1

1 Introduction

The increasing usage of electronics (including power electronics) is having a strong impact in the field of transportation, especially for the case of air transportation. This innovative scenario is motivating several companies in the aerospace industry to move towards the concept of more electric aircraft (MEA)[1)]. The key idea of the MEA essentially resides in replacing the heavy, leaky, hydraulic and pneumatic devices on-board aircraft with their electrically-driven counterparts. The advantages are several, such as increased fault-tolerance capability, size and weight reduction and, finally, pollution reduction. For example, replacing hydraulic actuators for the aircraft control surfaces with electromechanical (EMA) or electrohydrostatic (EHA) actuators [1], results in weight reduction, as the whole central hydraulic system can be removed, increased reliability, as a local fault has just a local effect and does not propagate along the actuators and/or supply pipe, and increased efficiency, typical of electric motors with respect to their hydraulic counterpart. In the past years, the achievement of these objectives has been strongly encouraged by several European framework programmes (FP). Starting from the fifth FP, where the concept was first explored with the POA project (power optimised aircraft)[2)], it has been investigated

* Corresponding author (email: alberto.cavallo@unicampania.it)

1) Mea info. http://www.moreelectricaircraft.com.

2) POA. Poa-power optimised aircraft project. http://www.2020-horizon.com/POA-Power-optimised-aircraft(POA)-s16028.html (2002-2005).

in depth with the MOET (more open electric technologies)[3] project and then, starting from FP7, with the creation of a joint undertaking named CleanSky, followed by CleanSky2 [4], that has become the largest European funder in aeronautic applications related to MEA activities. The rapidly increasing number of electric devices on-board, specifically, energy-storage devices [2, 3], has called for the need of advanced energy management techniques [4–9]. Moreover, increased usage of electric devices, jointly with "smart" materials, allows new achievements also on the structural part of the aircraft [10–12]. In this paper we consider the standard architecture, that is a simplified electric architecture consisting of a high voltage (HV) DC bus directly supplied by the main aircraft generator and a low voltage (LV) DC bus where a pack of batteries is placed. Specifically, on the HV side there is a 270 V generator undergoing a rectification, where heavy loads, e.g., electromechanical actuators, ice protection systems, air conditioning, cabin pressurisation systems, are connected. On the LV side instead, a pack of batteries resides [13, 14]. The standard power management requires the use of batteries only for special operations such as engine start-up, or an emergency electric source in case of generator fault. However, the usage of the battery pack can be rethought in order to fully exploit its capabilities. In fact, it would be convenient to use the power provided by the batteries also in non-critical situations, for instance in the case of an increased power demand by the loads connected to the electrical power grid for a limited amount of time [15, 16]. The standard approach to this problem is to design an over-sized generator in order to fulfill the power request in the case of occurrence of extra-load, while using the battery pack as a further power source would allow the installation of a smaller (hence lighter) generator on-board. It is known [17] that electric generators have the capability to supply current exceeding their nominal (rated) level during a short transient, so that if after this transient another device (e.g., a battery) can supply extra current, there is no need for increasing the rated power (and weight) of the generator. In fact, the generator sizing is based on the so-called "5-seconds" and "5-minutes" overload capability that is a simplified version (piecewise constant) of the generator true overload curve. Basically, the generator is usually able to fulfill a large overload for the first 5 s, so that, if before the 5 s elapse, the battery can supply the extra-load, then there is no need for generator over-sizing. The key element for power transfer among the HV and the LV sides is the DC-DC bidirectional buck-boost converter unit (BBCU) [18]. The choice of this type of converter is preferred above the usage of two converters (a buck and a boost converter) in order to save space and reduce cost and weight. The BBCU is used in order to revert the power flow in the two possible usage modes. Specifically, in nominal conditions, i.e., when the generator can feed the loads without exceeding its nominal current, the generator is responsible for feeding the load and charging the battery. When an overload occurs, instead, the battery may be charged with a lower current or, in case of heavy overload, the power flow must be reverted (by the BBCU) and the battery is called for helping the generator feeding the load. In this second scenario, after a short transient, the generator current cannot exceed its nominal current value. However, in a realistic approach, care must be taken for the battery state of charge (SoC). In fact, it is unrealistic to consider the battery pack being able to provide power for indefinitely long time intervals. When an overload occurs and the battery SoC drops below a certain threshold, priority to the battery recharging operation must be given (considering the battery key-role in acting as an additional power source in emergency cases). When such scenario occurs, a possible solution is the partial shedding of non-priority loads. The implementation of this idea needs two levels of control: a low level, aimed at precisely tracking current and voltage references [18], and a high level supervisor, switching among different control modes in order to achieve the control objectives in such a way that stability is ensured. With regards to the low level control, although several robust control techniques are available, most of them mainly refer to the case of linear systems (e.g., H_∞, μ-synthesis [19, 20]). Extension to the nonlinear case for H_∞ controllers has been proposed [21] but the design is rather complex, involving the solution of partial differential equations. A possible approach for resolving the nonlinear problem is to resort to linearisation with the known drawback of addressing only local behaviours. Among the several possible nonlinear control techniques, the one designed for this paper is the sliding mode control (SMC) [22, 23]. Moreover, because the BBCU are switching devices, sliding mode control seems to be the most suitable

3) Moet-more open electrical technologies. http://cordis.europa.eu/project/rcn/81472 (2006-2009).
4) Clean sky website. http://www.cleansky.eu/innovative-technologies (2010-2020).

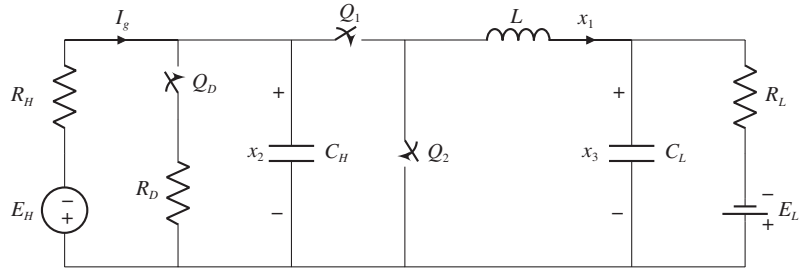

Figure 1 Bidirectional converter schematic.

control strategy given its property of outputting a discontinuous control signal [24–26]. However, one of the severe drawbacks of the SMC consists in the variable switching frequency of the control input, so in order to keep the commutation frequency fixed, pulse width modulation (PWM) implementation has also been proposed. In this paper, a high gain control based on sliding manifold (SHG) approach is used, resulting in a continuous control with robustness properties comparable to classical sliding mode [27,28]. Then, a standard PWM implementation is possible. Moreover, stability of the high level control must be ensured also. In this paper it will be shown how the stability requirement is achieved by resorting to the concept of a suitably defined dwell-time [29–31], by using the concept of common Lyapunov function (CLF) [32] for switched systems with multiple equilibrium points [33]. Finally, detailed simulations are performed by using SimPowerSystem MATLAB package and different operating conditions are considered.

2 System description and modelling

As mentioned in Section 1, the electric power grid considered in this paper presents the BBCU as a key device for the power transfer among the HV and LV sides. A 270VDC generator undergoing rectification resides on the HV side feeding large loads, while the LV side is characterized by the presence of a battery at a lower voltage. The power transfer is allowed through regulation of the BBCU's switches.

The topology of the BBCU bidirectional converter considered in this paper uses two capacitors and one inductor as shown in Figure 1. E_H represents the aircraft generator with its internal resistance R_H, while the battery is represented as an ideal voltage generator E_L with internal resistance R_L. Note that the battery has been modeled as an ideal voltage generator, which in certain working conditions, behaves similarly to a battery. It is clear that this model can be considered only when the battery is supplying the loads for a limited amount of time, as the battery discharge cannot be considered with this mode. For the discharge phenomenon we will consider detailed simulation components. The BBCU presents two capacitors, namely C_H and C_L, and an inductor L with Q_1 and Q_2 being the BBCU's switches operating in anti-phase. The total (active) load connected to the power grid is represented as the resistor R_D with Q_D being the switch responsible for the load power partial shedding. The model dynamic equations can be trivially derived by analysis of the four possible configurations, namely (Q_1 on, Q_2 off, Q_D off), (Q_1 off, Q_2 on, Q_D off), (Q_1 on, Q_2 off, Q_D on) and (Q_1 off, Q_2 on, Q_D on), and can be described in a compact way as

$$\dot{x}_1 = -\frac{1}{L}x_3 + \frac{1}{L}x_2 u, \tag{1}$$

$$\dot{x}_2 = -\left(\frac{1}{R_H} + w\frac{1}{R_D}\right)\frac{1}{C_H}x_2 - \frac{1}{C_H}x_1 u + \beta_H, \tag{2}$$

$$\dot{x}_3 = \frac{1}{C_L}x_1 - \frac{1}{R_L C_L}x_3 + \beta_L, \tag{3}$$

where $\beta_i = E_i/\left(R_i C_i\right), i \in \{L, H\}$ and the state variables assume the following meaning:

- x_1 is the current flowing through the inductor L;
- x_2 is the voltage on the HV capacitor C_H;
- x_3 is the voltage on the LV capacitor C_L.

The control inputs u and w are binary variables assuming discrete values in $\{0, 1\}$ and defining the four possible configurations. More precisely, $u = 0$ means Q_1 off and Q_2 on, and viceversa $u = 1$ stands for Q_1 on and Q_2 off while $w = 0$ means Q_D off and $w = 1$ indicates that Q_D is on.

As mentioned above, this model presents an ideal battery on the LV side, i.e., the battery will never discharge. Hence, in the following, the battery SoC will be considered as an external signal in this model.

3 Proposed control design

The proposed control consists of a hierarchical structure comprising a low level and a high level control. The low level control is responsible for driving the system state towards a control objective; the high level control, instead, is defined by a supervisor, implemented as a finite state automaton, which selects the appropriate control goal in order to satisfy the desired constraints of the system. Specifically, two low level control objectives can be selected: charging the battery with a constant current $\bar{x}_1$ [34, 35] or driving the HV capacitor voltage x_2 to a constant value $\bar{x}_2$ in order to limit the generator current to a prescribed value (I_{OL}). Imposing a fixed set-point on the generator current can be achieved by acting on the HV capacitor voltage because x_2 is related to the generator current I_g by a linear relationship, as it will be shown later.

3.1 Low level control

In order to ensure tracking of the variable x_1 to the reference $\bar{x}_1$, define a sliding manifold

$$\mathbb{S} = \{(t, x) | \sigma(t, x) = 0, \forall t \geqslant 0\}, \tag{4}$$

where the sliding function σ is

$$\sigma(t, x) = k(t)x_2 - x_1, \tag{5}$$

and $k(t)$ is a scalar smooth function. A suitable control strategy is to use a high gain PI controller to keep the controlled system state on the manifold. Note that, in order to avoid initial control peaks, one must select $k(0) = x_1(0)/x_2(0)$ so that $\sigma(0, x) = 0$. Moreover, with this choice of $k(0)$, there will be no transient phase for the reaching time on the manifold (4), or, more correctly, there is no reaching phase, as the system state starts on the manifold.

Theorem 1. Consider the system (1)–(3) and the control law

$$u(t) = \frac{1}{\epsilon}\left(\sigma(t, x) + c\int_0^t \sigma(\tau, x)\mathrm{d}\tau\right) \tag{6}$$

with $c, \epsilon > 0$. Let moreover $k(t) = k_0\mathrm{e}^{-\gamma t} + k_1$ with scalar constants k_0, k_1 and a positive constant γ, subject to constraints $k_0 + k_1 = x_1(0)/x_2(0)$ and $x_2(0) > 0$. Let $x(t, \epsilon)$ be the solution of system (1)–(3) with control law (6); then as $\epsilon \to 0$ the closed-loop system converges exponentially to a unique steady-state solution and

$$\lim_{\epsilon\to 0}\lim_{t\to\infty} |x_1(t, \epsilon) - k(t)x_2(t, \epsilon)| = 0. \tag{7}$$

Proof. The proof of this theorem follows the same steps as in [36] and it is based on the theory of singular perturbations on the infinite time horizon [37]. For the sake of completeness, we give here a sketch of the proof. It is trivial to prove that the control law (6) results from the solution of the differential equation

$$\epsilon\dot{u} = \dot{\sigma} + c\sigma. \tag{8}$$

Resorting to the theory of singular perturbations and to Tikhonov's theorem on the infinite time horizon, let $\epsilon = 0$ and solve (8) for u, obtaining the so-called equivalent control

$$u_0 = \frac{L}{(Lk(t)^2 + C_H)x_{20}}\left\{\left[\dot{k}(t) + \left(\frac{1}{R_H} + \frac{1}{R_D}\right)k(t)\right]x_{20} + x_{30}L + \beta_H k(t)\right\}. \tag{9}$$

Replacing the equivalent control in (2) and (3), the resulting linear time-varying system (reduced order system) is

$$\dot{\bar{x}}_0 = (A_1 + A_2(t)\mathrm{e}^{-\gamma t})\bar{x}_0 + (B_1 + B_2(t)\mathrm{e}^{-\gamma t})v, \tag{10}$$

where $\bar{x}_0 = [x_{20}, x_{30}]^{\mathrm{T}}$, the subscript stands for the solution with $\epsilon = 0$ and $v = [E_H, E_L]^{\mathrm{T}}$, and the matrices A_1 and B_1 are

$$A_1 = \begin{bmatrix} -\frac{\frac{1}{R_H}+\frac{1}{R_D}}{Lk_1^2+C_H} & -\frac{k_1}{Lk_1^2+C_H} \\ \frac{k_1}{C_L} & -\frac{1}{R_L C_L} \end{bmatrix}, \tag{11}$$

$$B_1 = \begin{bmatrix} \frac{1}{R_H(Lk_1^2+C_H)} & 0 \\ 0 & \frac{1}{R_L C_L} \end{bmatrix}. \tag{12}$$

The proof of Theorem 1 in [36] shows that the reduced order system is stable. Finally the theory of singular perturbations on the infinite time horizon guarantees that closed-system loop is exponentially stable for $\epsilon \to 0$.

Remark 1 (Selection of k_1)**.** Note that, owing to the choice of the sliding function in (5), the equivalent system (10) has become linear. According to the control objective, i.e., charging the battery with a constant prescribed current or controlling the generator current to a limited prescribed value, the control parameter k_1 has to be chosen. Specifically, if

$$k_1 = \frac{E_H - \sqrt{E_H^2 - 4R_H^2\bar{x}_1(R_L\bar{x}_1 + E_L)(\frac{1}{R_H}+\frac{1}{R_D})}}{2R_H(R_L\bar{x}_1 + E_L)}, \tag{13}$$

then

$$\lim_{t\to\infty} x_1(t) = \bar{x}_1. \tag{14}$$

Hence the battery will be charged with a constant current $\bar{x}_1$. If

$$k_1 = \frac{-E_L + \sqrt{E_L^2 - 4R_L\bar{x}_2((\frac{1}{R_H}+\frac{1}{R_D})\bar{x}_2 - \frac{E_H}{R_H})}}{2R_L\bar{x}_2}, \tag{15}$$

then

$$\lim_{t\to\infty} x_2(t) = \bar{x}_2 \tag{16}$$

and the generator current will reach a constant value depending on $\bar{x}_2$ due to

$$I_g = \frac{E_H - x_2}{R_H}. \tag{17}$$

These results are shown in a more accurate fashion in [36].

Remark 2. Note that in order to compute k_1 in (13) or in (15) the value of the uncertain load R_D must be known or estimated. This has been done in [36] using a Levant finite-time differentiator [38]. However, the effectiveness of the solution still depends on the knowledge of all the remaining parameters of the system. An alternative solution has been proposed in [35], where a machine learning approach based on decision trees has been considered. This solution is also robust against plant parameter uncertainties, because it is based on a classification of the signals in the circuit, not on the accuracy of the mathematical model. Another approach is to use a disturbance observer [39, 40] to reduce the effect of unknown parameters and external disturbances. A further approach, currently under investigation, is the use of adaptive strategies for the gain k.

Remark 3. In the definition of k, the initial state is assumed to be known. As the state is measured at any time, this is a reasonable assumption. However, in some application the initial value of the state may be unknown, and this would result in an initial peak in the control. A way to alleviate this is to consider a rate-limited high-gain controller [41]. Details are not given here.

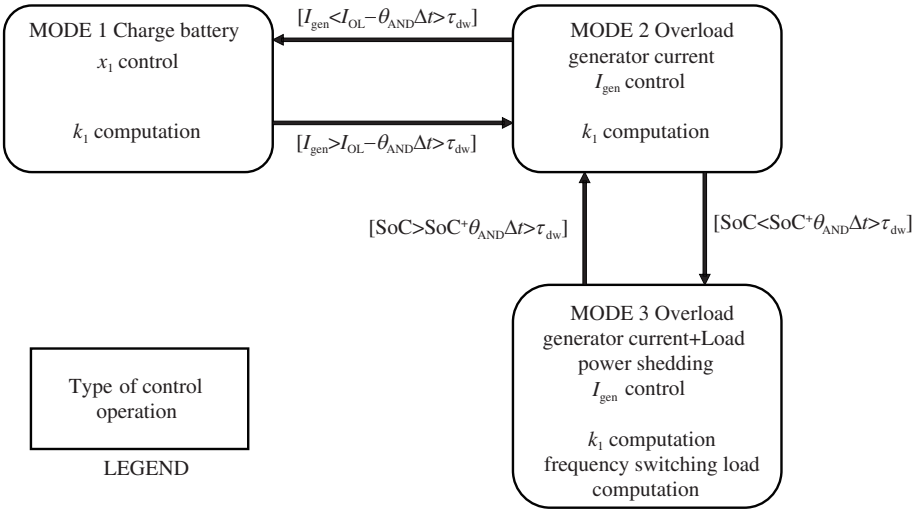

Figure 2 Supervisor scheme.

3.2 High level control

The high level control is demanded for the proper selection of the control objectives. More precisely, it aims at detecting two unusual conditions, i.e., the generator overload and the battery SoC dropping below a certain threshold, and selects the proper low level control strategy in order to satisfy the desired constraints of the system. This high level control paradigm can be implemented by a supervisor with three operational modes (Figure 2):

• MODE 1. This is the nominal operational mode in which the generator on the HV side feeds the load and, at the same time, charges the battery with a constant current $\bar{x}_1$. Parameter k_1 is chosen according to (13).

• MODE 2. This operational mode is selected when more loads are connected to the power grid, thus requiring a higher generator current. In this case, the generator current is set to a fixed set-point and two possible scenarios can arise:

(1) The generator can still feed both the loads and the battery (but with a current lower than $\bar{x}_1$);

(2) The battery is asked to help the generator with feeding the load with the required power.

In both cases, the control parameter k_1 is chosen according to (15).

• MODE 3. During the overload condition the battery may be discharging (i.e., when the supervisor is in the second case of MODE 2). This mode is entered when the battery SoC drops below a certain threshold SoC^-. In this scenario the controller performs a control action on the switch Q_D in order to increase the resistance seen by the generator. Specifically, the equivalent resistance seen by the generator is equal to

$$\hat{R}_D = \frac{R_D}{w}, \tag{18}$$

where the control input w is regulated in order to obtain a prescribed value of the equivalent resistance. The supervisor leaves MODE 3 when the battery SoC reaches an upper threshold, namely SoC^+.

However, it is well known that switching between operational modes may cause instability of the system [42]; therefore, stability of the switched system must be proven. In order to avoid chattering between MODE 1 and MODE 2, the commutation takes place with hysteresis on the generator current with band $[I_{\mathrm{OL}} - \theta, I_{\mathrm{OL}} + \theta]$, while chattering avoidance between MODE 2 and MODE 3 is assured by setting the two switching points (i.e., SoC^+ and SoC^-) sufficiently far from each other. However, in order to prove the stability of the switching system, the computation of a minimum dwell-time is required [36, 43]. Note that the definition itself of the hysteresis introduces a minimum dwell-time. Moreover, owing to the choice of $k_0 + k_1 = x_1(0)/x_2(0)$, the system trajectories belong to the manifold at every switching instant, therefore no reaching time computation is needed. While sliding along the

manifold, the system trajectories assume the form (10) which is a second order linear time-varying system. However, in [36] it is proven that the elements of matrices $A_2(t)$ and $B_2(t)$ are bounded, hence the time-varying contribute of (10) can be neglected by choosing γ appropriately large. System switching occurs either when there is a load variation or a supervisor mode variation. In the former case, the parameters R_D and k_1 in the matrices A_1 and B_1 respectively from (11) and (12) change, while in the latter case only k_1 undergoes a variation. Stability of the switching system can be investigated considering a discrete set of admissible loads or a discretization of a continuous range of loads; hence, we need to investigate the stability problem for the switching system

$$\dot{\xi} = A_i\xi + B_i v, \qquad i \in [1, \ldots, m] \tag{19}$$

with A_i and B_i being the matrices obtained for each selection of R_D.

Theorem 2. Consider the switched LTI systems (19). Assume each $A_i \in \mathbb{R}^{n\times n}$ Hurwitz, let $\bar{\xi}_i = -A_i^{-1}B_i v$ be the equilibrium point of each system, and let $P \succ 0$ be the solution of the linear matrix inequality problem

$$A_i^{\mathrm{T}}P + PA_i \prec -I. \tag{20}$$

Denote $\bar{\theta}_M = \max_{i,j}\left(\bar{\xi}_i - \bar{\xi}_j\right)^{\mathrm{T}} P\left(\bar{\xi}_i - \bar{\xi}_j\right)$, $i, j \in [1, \ldots, m]$. Then for any given $l > 0$ and every switching between systems of the family (19) with dwell time

$$\tau > 2\lambda_{\max}(P)\ln\left(1 + \sqrt{\frac{\bar{\theta}_M}{l}}\right), \tag{21}$$

the trajectory of the switching system is bounded.

Proof. The proof is based on Theorem 1 in [33]. Essentially, m Lyapunov functions are defined, i.e.,

$$V_i = (\xi - \bar{\xi}_i)^{\mathrm{T}}P(\xi - \bar{\xi}_i), \qquad i \in [1, \ldots, m] \tag{22}$$

for each subsystems of the switched system. Then it is easy to show that, owing to the solution of the LMI (20),

$$\dot{V}_i \leqslant -\epsilon V_i \tag{23}$$

with the same $\epsilon = 1/\lambda_{\max}(P)$. Moreover, define the sets $\mathcal{N}_i = \{\xi \in \mathbb{R}^n | V_i(\xi) \leqslant l\}$, along with the set

$$\mathcal{M} = \bigcup_{i\in[1,\ldots,m]} \{\xi \in \mathbb{R}^n | V_i(\xi) \leqslant \rho\} \tag{24}$$

with

$$\rho = \left(\sqrt{l} + \sqrt{\bar{\theta}_M}\right)^2. \tag{25}$$

Then Theorem 1 in [33] shows that for any initial condition, there exists a $T > 0$ such that after T the state of the switching system enters one of the sets $\mathcal{N}_i$, and remains in $\mathcal{M}$. Thus, in any case the trajectory of the switching system is bounded.

Remark 4. Note that the parameter l from (21) can be chosen in order to improve the precision of the behaviour of the switching system in terms of distance from the equilibrium point of any linear system before next switch happens. In fact, a higher value of l corresponds to a smaller dwell-time, and vice versa, a small l implies a larger dwell-time.

Theorem 2 will be used to define the dwell-time that the supervisor must wait before allowing further commutations. The above theoretical results are the basis for the design of a hierarchical controller aimed at the management of the battery operations, as it will be shown in the next section.

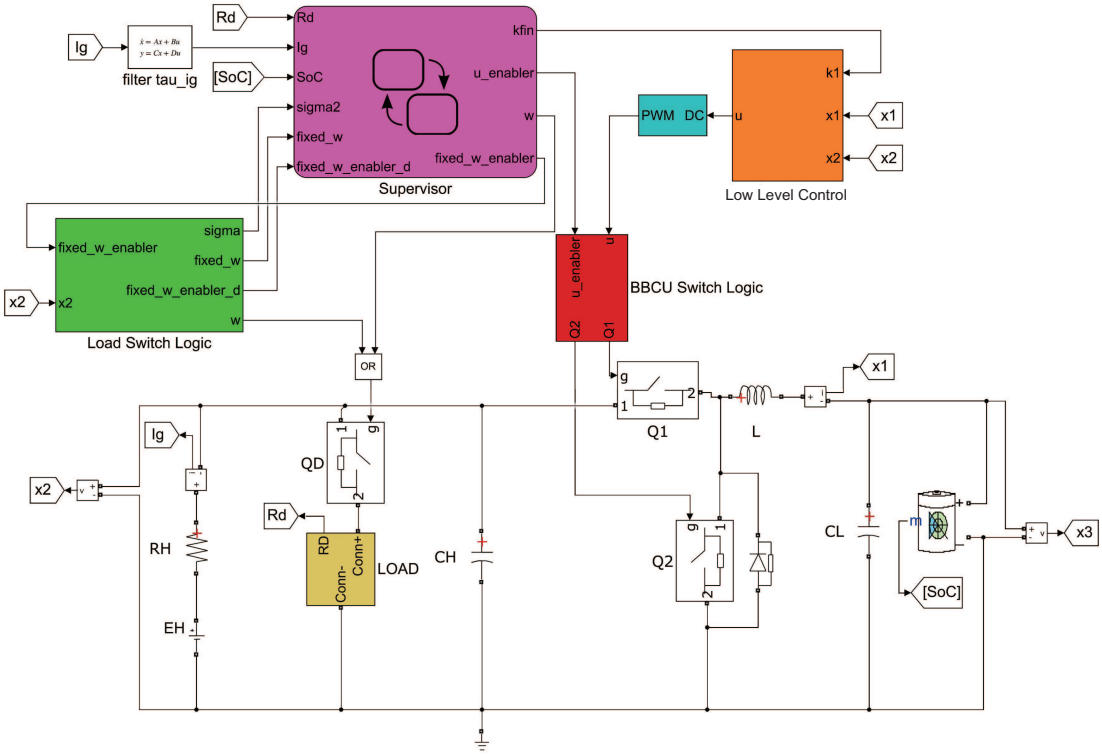

Figure 3 (Color online) Detailed simulation scheme.

4 Simulation results

A detailed MATLAB/Simulink/SimPowerSystem simulator (Figure 3) has been implemented in order to demonstrate the effectiveness of the control strategy proposed in the previous section. The simulator presents detailed model of the switching devices and of the battery, available in the detailed models library of SimPowerSystem, which allows the management of the SoC. In particular, the battery is not an ideal voltage source, but an NiCd battery with nominal voltage 24 V, as in standard practice [44], has been considered. The simulator is made of five blocks:

- LOAD: contains a bank of parallel resistors R_{D_i}, which can be individually connected to the circuit (yellow block).
- LOAD SWITCH LOGIC: is responsible for the switching logic of the switch Q_D (green block) called for load power shedding.
- BBCU SWITCH LOGIC: enables the switching of Q_1 and Q_2 (red block).
- PWM: is pulse-width modulation (cyan block).
- SUPERVISOR: implements the high level control according to Subsection 3.2 (magenta block).
- LOW LEVEL CONTROL: implements the low level control based on SHG strategy according to Subsection 3.1 (orange block).

The system and controller parameters considered in the simulations campaign are shown in Tables 1 and 2.

It must be noted that, in order to filter the generator current in the switching implementation, a first order filter

$$F(s) = \frac{1}{\tau_g s + 1}, \tag{26}$$

where $\tau_g = 0.01$ s is used. Although the presence of filter induces a delay, it is short enough that it can be considered negligible, as shown in the simulations. As mentioned previously, in order to ensure the stability of the switched system, the dwell-time has been computed. Specifically, 100 different loads R_D

Table 1 Simulation parameters

Parameter	Value	Unit	Parameter	Value	Unit
E_L	28	V	C_L	400	μF
E_H	270	V	R_H	100	mΩ
L	10	mH	R_L	280	mΩ
C_H	800	μF			

Table 2 Controller parameters

Name	Value	Unit	Name	Value	Unit
ϵ	0.1	A^{-1}	$\bar{x}_1$	10	A
c	1	s^{-1}	θ	0.5	A
γ	30	s^{-1}	SoC^+	55%	–
I_{OL}	16	A	SoC^-	50%	–

Table 3 BBCU data

Parameter	Resistance (Ω)	Activation time (s)
R_{D_1}	300	[0,30) [190 200]
R_{D_2}	16.8	[30,60)
R_{D_3}	16	[60,190)

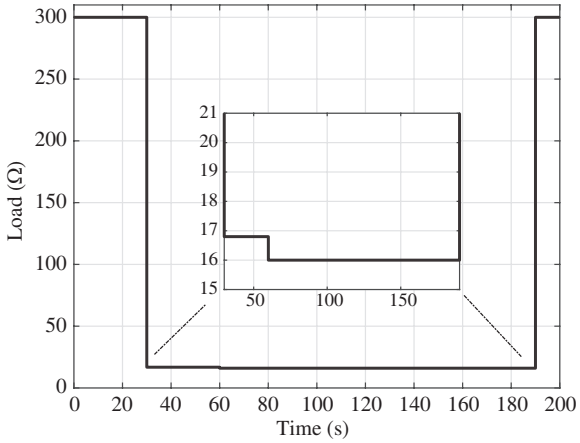

Figure 4 Load variation for scenario 1.

have been considered in the interval $[16, \ldots, 320]$ Ω and the dwell-time has been calculated following the results of Theorem 2. In the specific case, the dwell-time obtained is $\tau_{\mathrm{dw}} = 23.1$ μs that is small enough to be neglected. Note that in this case we have no approximation. We are mathematically sure that in this application switching among different modes can make no harm. Moreover, the input signal is generated by a PWM at a constant frequency of 200 kHz. Finally, in order to widely test the behaviour of the controlled system, two different simulation scenarios have been implemented.

4.1 Scenario 1

The first scenario presents a load variation as in Figure 4 with load variations and activation times as in Table 3.

Initially, a rather light load (R_{D_1}) is connected to the power grid. Such a load does not establish an overload condition; therefore the battery can be charged with a constant current $\bar{x}_1$ and at the same time the generator current is kept below the threshold I_{OL}. Next, one more load, R_{D_2} is added, resulting in generator overload. Then, automatically the current charging the battery is reduced, as apparent in the slope of the battery SoC in Figures 5(a) and (b) with reference to the current charging the battery which is still positive but lower than the prescribed constant $\bar{x}_1$.

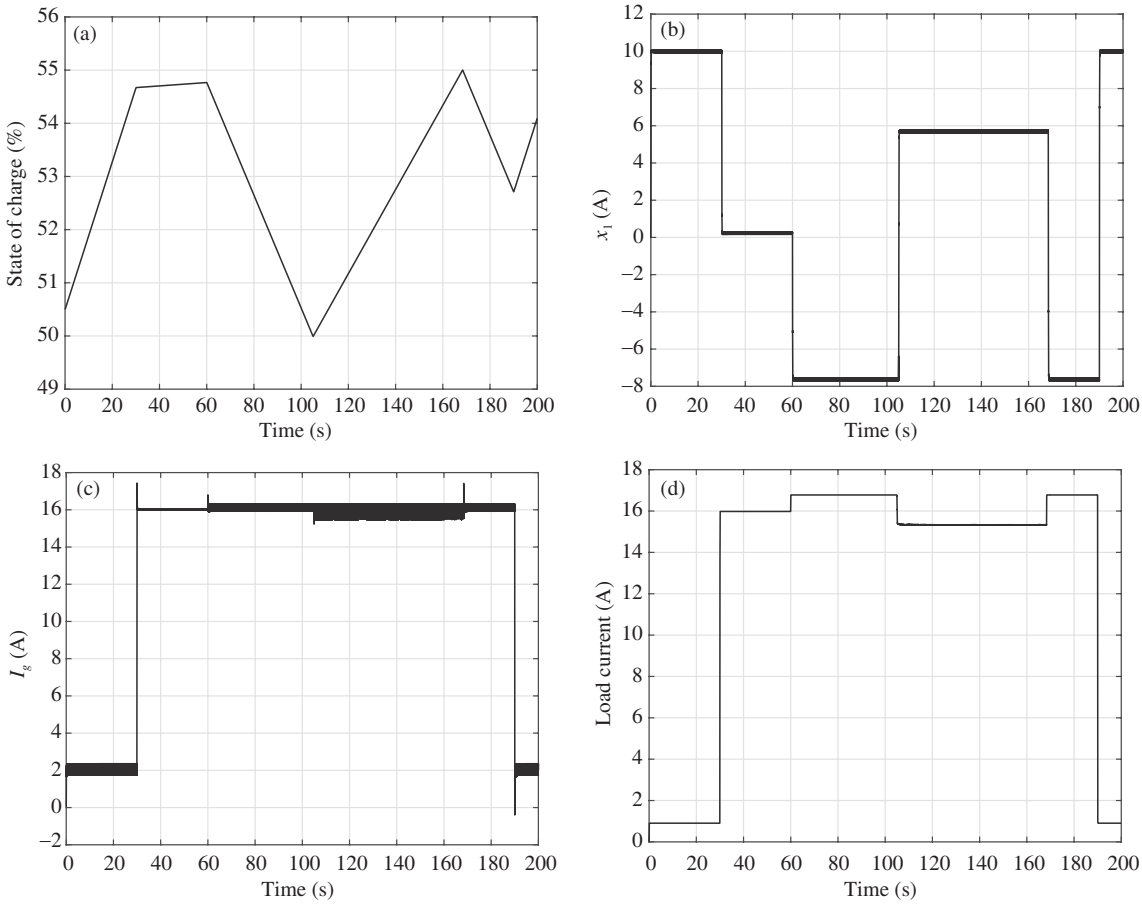

Figure 5 Battery state of charge (a), inductor current (b), generator current (c), and load current (d) of Scenario 1.

The generator current is presented in Figure 5(c), showing that in this phase, after a short transient, the generator current is fixed at the overload value. At $t = 60$ s load R_{D_3} is inserted. In this case the generator overload cannot be solved even by disconnecting the battery. Then the battery is called for helping the generator in supplying the load, as apparent from the sign of the inductor current in Figure 5(b), that is reversed, and by the SoC of the battery in Figure 5(a), that decreases. After some amount of time, at about $t = 105$ s, the SoC reaches its lowest allowed level (namely SoC^-), and then the supervisor enters MODE 3, modulating the switch Q_D and thus reducing the power to the load (that is assumed to be a low priority load). This action is apparent in Figure 5(d), showing the reduction in the load current. So an extra-power from the generator is now available to recharge the battery up to SoC^+. After this event, the supervisor exits MODE 3 and enters MODE 2, and the full load is restored, with the battery helping the generator. Finally, at $t = 190$ s, the initial load configuration occurs, and the initial working conditions are automatically executed. Robustness of the proposed strategy is evident in Figures 5(b) and (c), showing the correct tracking of battery current ($\bar{x}_1$) and generator current (I_{OL}) also in the presence of load variation. Note that in this simulation the time for the discharge of the battery is not realistic. It has been exaggerated in order to reduce simulation times. Finally, the bus voltages have been plotted in order to show their compliance with the aeronautical standards (see MIL-STD-704F [45]). The MIL standard defines steady-state and transient bounds that the voltage must fulfil. In particular, in Figure 6(a) the bounds for the low-voltage 28VDC bus is shown, showing that voltages in the interval $[22, 29]$ V are admissible in steady-state, and a larger range can be tolerated for a short 80 ms transient. Similarly, Figure 6(b) shows the aeronautical standards for high voltage (270VDC) in transient and steady-state phase.

Comparison of Figures 6(a), (c) and Figures 6(b), (d) shows that low and high voltages busses are definitely within the limits both in the transient and in steady-state phase.

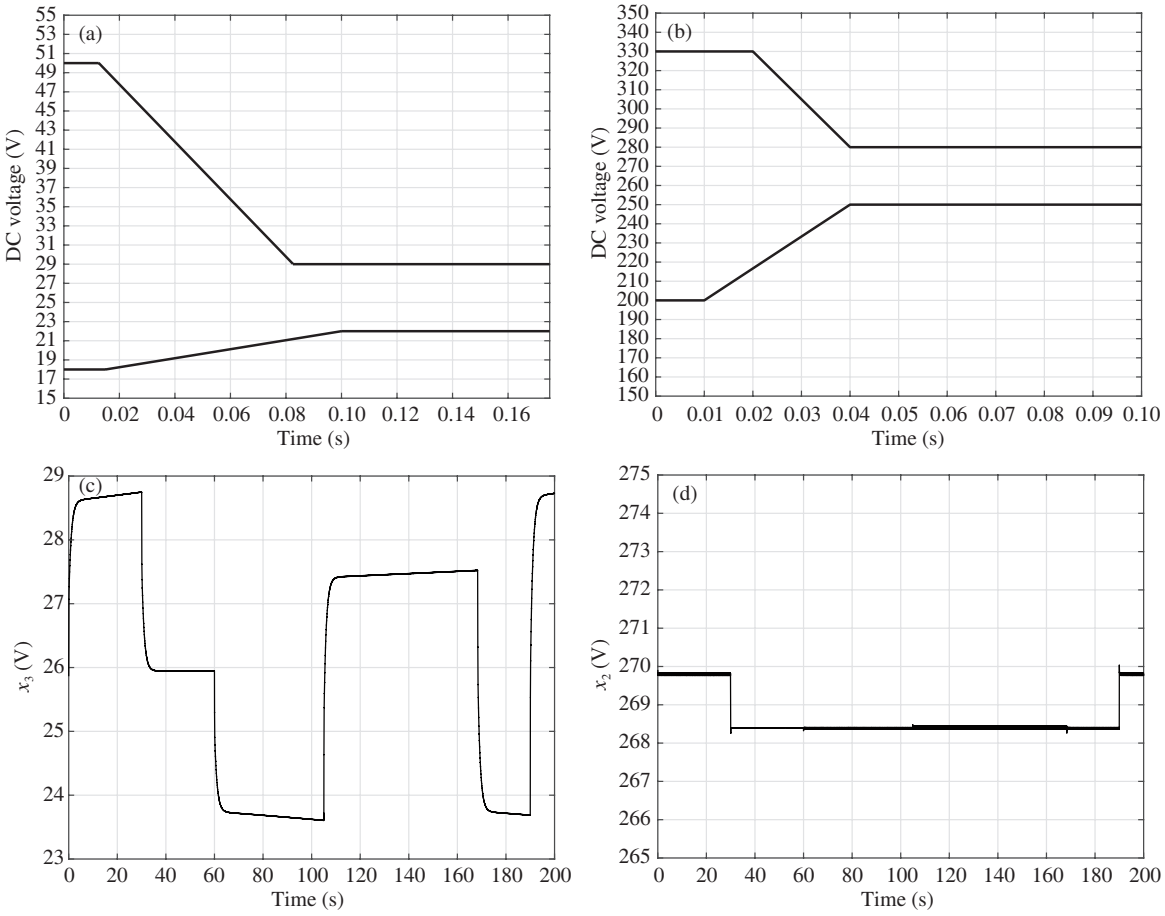

Figure 6 (a) LOW voltage (LV) bus MIL limits, (b) HIGH voltage (HV) bus MIL limits, (c) LV bus, and (d) HV bus.

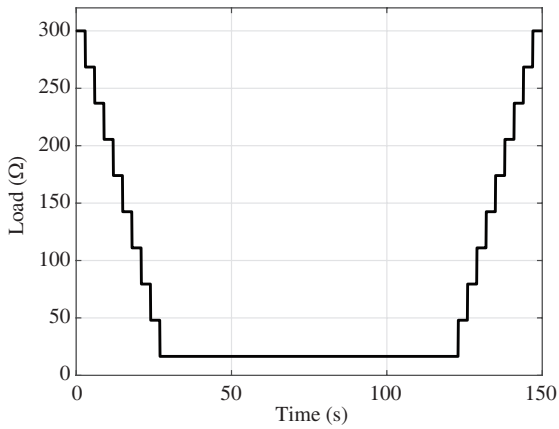

Figure 7 Load variation for Scenario 2.

4.2 Scenario 2

The second scenario presents a sudden load variation as in Figure 7 with load changing from 300 to 16.5 Ω.

At the beginning of the simulation, the Supervisor is in MODE 1 with load $R_D = 300$ Ω; therefore the goal is to drive x_1 to $\bar{x}_1 = 10$ A. Also in this case the battery SoC starts from 50.5%. Figure 8(a) shows that the initial battery current is $x_1(0) = 5$ mA and quickly reaches the reference. The load decrease is of 31.5 Ω every 3 s until $t = 30$ s. Figure 8(b) shows the load current. In this time interval the system

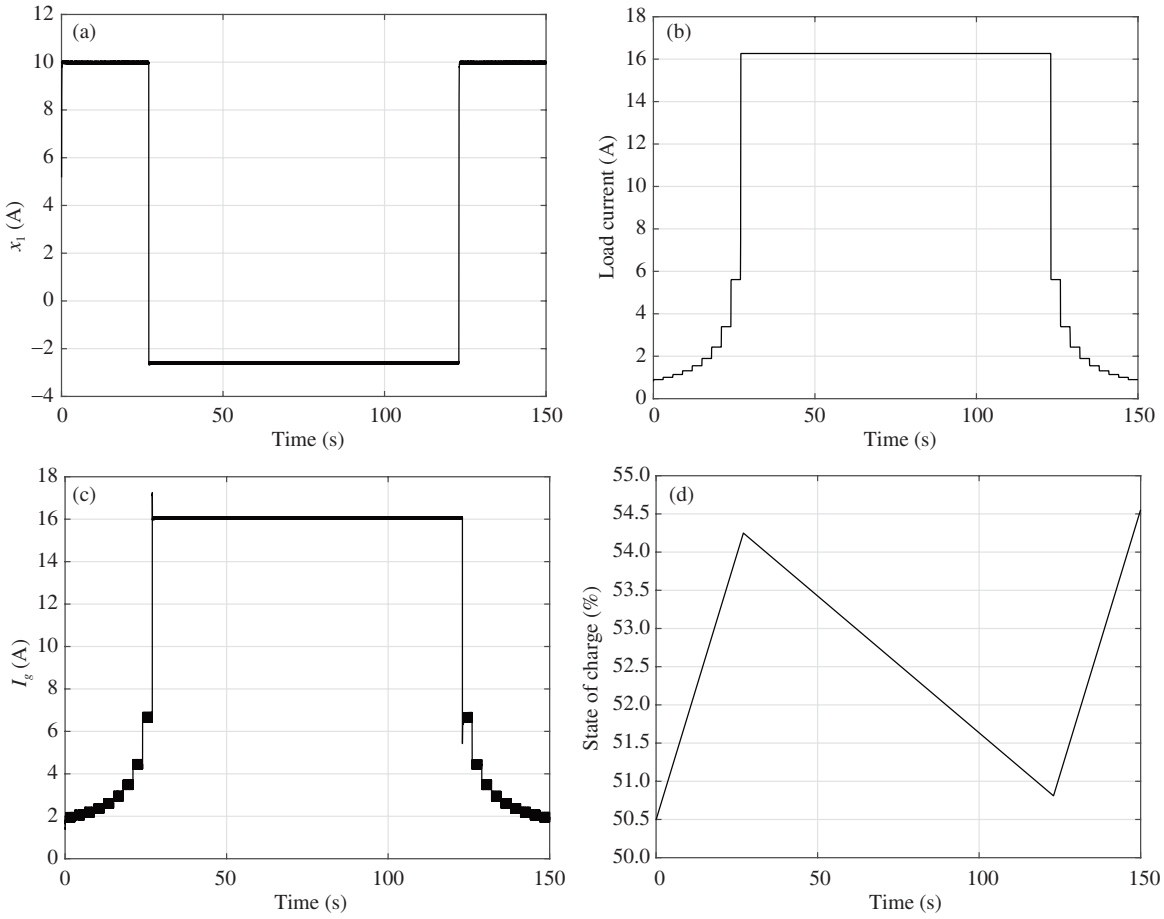

Figure 8 Inductor current (a), load current (b), generator current (c), and battery state of charge (d) of Scenario 2.

remains in MODE 1. At time instant $t = 30$ s a new load is added, resulting in a reduction of total load resistance to $R_D = 16.5\ \Omega$. In this case the overload capacity of the generator is exceeded; hence the supervisor switches to MODE 2. The new objective is to keep I_g to I_{OL}, as Figure 8(c) shows. Next, at $t = 120$ s the load changes again to 48 Ω. Now the generator is no longer able to supply the battery, and the inductor current changes sign; i.e., the battery helps the generator to supply the loads. Finally the load resistance increases of 31.5 Ω every 3 s until 150 s, so it returns to its initial condition of 300 Ω, and the controller automatically recovers its initial state. Figure 8(d) shows the state of charge of the battery during the simulation. For the sake of simplicity, the low and high-voltage busses are not showed, but also in this case they are kept within the bounds of aeronautical standards.

5 Conclusion

This paper presented the design of a hierarchical control based on sliding mode aimed at the implementation of energy management rules for aeronautic applications. The strategy described above consists in transferring the energy from the HV side, where the generator resides, to the LV side, where a battery is placed. Energy transfer is achieved through the action of a BBCU in order to accomplish the dual objective of keeping the generator current below a certain threshold and, at the same time, keeping the battery SoC above a lower threshold. The control strategy used is defined at two levels. In a low-level approach a sliding surface is defined, chosen so that as the controlled state belongs to the surface, the overall controlled system behaves like a linear system. The controller used to drive the system state on the sliding manifold is a high-gain PI (proportional-integral) control, whose stability has been rigorously proved. The low-level approach basically forces the converter current to track a desired reference. At

the high-level, a supervisory strategy is employed to switch between different operating modes. Also in this case the problem of stability between switching configurations is addressed and tackled by using a dwell-time concept. The objectives of the supervisor are basically keeping the battery charged and the generator away from the overload. In some critical cases (e.g., severe overload), it is not possible to fulfil the above requirement. In this case a further operational mode, i.e., a load power shedding technique is adopted. The results of the proposed strategy are currently the object of different research projects funded by the EU. Moreover, the results of a simulation campaign have been presented in order to prove the correctness and effectiveness of the control algorithm. Two scenarios are considered and detailed simulators are employed in order to test the effectiveness of the proposed approach. Further research will move towards the adoption of an adaptive control strategy in order to increase the robustness against uncertainties in the model, perhaps considering higher order sliding mode algorithms.

Acknowledgements This work was partially supported by ENIGMA (Grant No. 785416).

References

1 Maldonado M A, Shah N M, Cleek K J, et al. Power management and distribution system for a more-electric aircraft (madmel)-program status. In: Proceedings of the 31st Intersociety Energy Conversion Engineering Conference, 1996. 148–153
2 Buonanno A, Sparaco E, Cavallo A, et al. Rate- limiter control comparison for energy storage systems in aerospace applications. In: Proceedings of the 8th International Conference on Power Electronics, Machines and Drives, 2016
3 Cavallo A, Canciello G, Russo A. Supervised energy management in advanced aircraft applications. In: Proceedings of 2018 European Control Conference (ECC), 2018. 2769–2774
4 Cavallo A, Guida B. Power management of DC aeronautical electrical networks including supercapacitors. In: Proceedings of IEEE International Conference on Industrial Technology (ICIT), 2015. 2015–2020
5 Canciello G, Cavallo A, Guida B. Control of energy storage systems for aeronautic applications. J Control Sci Eng, 2017, 2017: 1–9
6 Canciello G, Cavallo A, Guida B. Robust control of aeronautical electrical generators for energy management applications. Int J Aerospace Eng, 2017, 2017: 1–12
7 Canciello G, Russo A, Guida B, et al. Supervisory control for energy storage system onboard aircraft. In: Proceedings of 2018 IEEE International Conference on Environment and Electrical Engineering and 2018 IEEE Industrial and Commercial Power Systems Europe, 2018. 1–6
8 Cavallo A, Canciello G, Russo A. Buck-boost converter control for constant power loads in aeronautical applications. In: Proceedings of 2018 IEEE Conference on Decision and Control (CDC), 2018. 6741–6747
9 Guida B, Cavallo A. A petri net application for energy management in aeronautical networks. In: Proceedings of IEEE 18th Conference on Emerging Technologies Factory Automation (ETFA), 2013. 1–6
10 Canciello G, Cavallo A. Selective modal control for vibration reduction in flexible structures. Automatica, 2017, 75: 282–287
11 Cavallo A, de Maria G, Natale C, et al. H_∞ strongly stabilizing bandpass controllers for flexible systems. In: Proceedings of the IEEE Conference on Decision and Control, 2006. 6543–6548
12 Cavallo A, de Maria G, Natale C, et al. Robust control of flexible structures with stable bandpass controllers. Automatica, 2008, 44: 1251–1260
13 Tooley M. Aircraft Electrical and Electronic Systems: Principles Maintenance and Operation. Oxford: Butterworth-Heinemann, 2009
14 Cavallo A, Canciello G, Guida B. Energy storage system control for energy management in advanced aeronautic applications. Math Problems Eng, 2017, 2017: 1–9
15 Cavallo A, Canciello G, Guida B. Supervised control of buck-boost converters for aeronautical applications. Automatica, 2017, 83: 73–80
16 Cavallo A, Guida B, Buonanno A, et al. Smart buck-boost converter unit op- erations for aeronautical applications. In: Proceedings of the 54th IEEE Conference on Decision and Control (CDC), 2015. 4734–4739
17 Ghosh S. Electrical Machines. 2nd ed. Delhi: Pearson Education, 2012
18 Cavallo A, Guida B. Sliding mode control for DC/DC converters. In: Proceedings of IEEE 51st Annual Conference on Decision and Control (CDC), 2012. 7088–7094
19 Zhou K, Doyle J. Essentials of Robust Control. Upple Saddle River: Prentice Hall International, 1998
20 Skogestad S, Postlethwaite I. Multivariable Feedback Control: Analysis and Design. Hoboken: John Wiley & Sons, 2005
21 Helton J, James M. Extending H-infinity Control to Nonlinear Systems: Control of Nonlinear Systems to Achieve Performance Objectives. Philadelphia: Society for Industrial and Applied Mathematics, 1999
22 Utkin V I. Sliding Modes in Control Optimization. Berlin: Springer-Verlag, 1992
23 Kosaraju K C, Cucuzzella M, Pasumarthy R, et al. Differentiation and passivity for control of brayton-moser systems. 2018. arXiv:1811.02838
24 Canciello G, Cavallo A, Cucuzzella M, et al. Fuzzy scheduling of robust controllers for islanded DC microgrids

applications. Int J Dynam Control, 2019, 57: 1–11
25 Cucuzzella M, Rosti S, Cavallo A, et al. Decentralized sliding mode voltage control in dc microgrids. In: Proceedings of 2017 American Control Conference (ACC), 2017. 3445–3450
26 Cucuzzella M, Lazzari R, Trip S, et al. Sliding mode voltage control of boost converters in DC microgrids. Control Eng Practice, 2018, 73: 161–170
27 Cavallo A, de Maria G, Nistri P. A sliding manifold approach to the feedback control of rigid robots. Int J Robust Nonlin Contr, 1996, 6: 501–516
28 Cavallo A, Natale C. Output feedback control based on a high-order sliding manifold approach. IEEE Trans Automat Contr, 2003, 48: 469–472
29 Lin H, Antsaklis P J. Stability and stabilizability of switched linear systems: a survey of recent results. IEEE Trans Automat Contr, 2009, 54: 308–322
30 Rejeb J B, Morărescu I, Girard A, et al. Design of O(ϵ) dwell-time graph for stability of singularly perturbed hybrid linear systems. In: Proceedings of 2017 American Control Conference (ACC), 2017. 1193–1198
31 Chesi G, Colaneri P, Geromel J C, et al. A nonconservative LMI condition for stability of switched systems with guaranteed dwell time. IEEE Trans Automat Contr, 2012, 57: 1297–1302
32 Shorten R N, Narendra K S. On common quadratic lyapunov functions for pairs of stable LTI systems whose system matrices are in companion form. IEEE Trans Automat Contr, 2003, 48: 618–621
33 Dorothy M, Chung S J. Switched systems with multiple invariant sets. Syst Contr Lett, 2016, 96, 103–109
34 Armstrong S, Glavin M E, Hurley W G. Comparison of battery charging algorithms for stand alone photovoltaic systems. In: Proceedings of 2008 IEEE Power Electronics Specialists Conference, 2008. 1469–1475
35 Cavallo A, Canciello G, Guida B, et al. Multi-objective supervisory control for DC/DC converters in advanced aeronautic applications. Energies, 2018, 11: 1–22
36 Cavallo A, Canciello G, Guida B. Supervisory control of DC-DC bidirectional converter for advanced aeronautic applications. Int J Robust Nonlin Control, 2018, 28: 1–15
37 Hoppensteadt F C. Singular perturbations on the infinite interval. Trans Amer Math Soc, 1966, 123: 521–535
38 Levant A. Higher-order sliding modes, differentiation and output-feedback control. Int J Control, 2003, 76: 924–941
39 Zhang Z, Wang F, Guo Y, et al. Multivariable sliding mode backstepping controller design for quadrotor UAV based on disturbance observer. Sci China Inf Sci, 2018, 61: 112207
40 Park G, Shim H. Guaranteeing almost fault-free tracking performance from transient to steady-state: a disturbance observer approach. Sci China Inf Sci, 2018, 61: 070224
41 Cavallo A, de Maria G, Nistri P. Robust control design with integral action and limited rate control. IEEE Trans Automat Contr, 1999, 44: 1569–1572
42 Branicky M S. Multiple Lyapunov functions and other analysis tools for switched and hybrid systems. IEEE Trans Automat Contr, 1998, 43: 475–482
43 Hespanha J P, Morse A S. Stability of switched systems with average dwell-time. In: Proceedings of the 38th IEEE Conference on Decision and Control, 1999. 2655–2660
44 Tariq M, Maswood A I, Gajanayake C J, et al. Aircraft batteries: current trend towards more electric aircraft. IET Electr Syst Transport, 2017, 7: 93–103
45 Department of Defense Interface Standards. Aircraft Electric Power Characteristics. MIL-STD-704F. 2004